Bioactive Materials 7 (2022) 217–226

Contents lists available at ScienceDirect

Bioactive Materials

journal homepage: www.sciencedirect.com/journal/bioactive-materials

The effect of enzymes on the in vitro degradation behavior of Mg alloy wires in simulated gastric fluid and intestinal fluid

Yue Zhang [a,b,c,1], Jian Cao [d,1], Xianli Wang [a,b], Huan Liu [e], Yi Shao [a,b,c], Chenglin Chu [a,b], Feng Xue [a,b], Jing Bai [a,b,c,*]

[a] School of Materials Science and Engineering, Southeast University, Jiangning, Nanjing 211189, Jiangsu, China
[b] Jiangsu Key Laboratory for Advanced Metallic Materials, Jiangning, Nanjing 211189, Jiangsu, China
[c] Institute of Biomedical Devices (Suzhou), Southeast University, Suzhou 215163, Jiangsu, China
[d] Peking University People's Hospital, Xi Cheng, Beijing 100044, China
[e] College of Mechanics and Materials, Hohai University, Nanjing, 211100, China

ARTICLE INFO

Keywords:
Degradable Mg alloy
Pepsin
Pancreatin
Gastrointestinal
Digestive tract

ABSTRACT

With an upsurge of biodegradable metal implants, the research and application of Mg alloys in the gastrointestinal environment of the digestive tract have been of great interest. Digestive enzymes, mainly pepsin in the stomach and pancreatin in the small intestine, are widespread in the gastrointestinal tract, but their effect on the degradation of Mg alloys has not been well understood. In this study, we investigated the impacts of pepsin and pancreatin on the degradation of Mg-2Zn alloy wires. The results showed that the pepsin and pancreatin had completely different even the opposite effects on the degradation of Mg, although they both affected the degradation product layer. The degradation rate of Mg wire declined with the addition of pepsin in simulated gastric fluid (SGF) but rose with the addition of pancreatin in simulated intestinal fluid (SIF). The opposite trends in degradation rate also resulted in completely different degradation morphologies in wires surface, where the pitting corrosion in SGF was inhibited because of the physical barrier effect of pepsin adsorption. In contrast, the adsorption of pancreatin affected the integrity of magnesium hydrogen phosphate film, causing a relatively uneven degraded surface. These results may help us to understand the role of different digestive enzymes in the degradation of magnesium and facilitate the development and clinical application of magnesium alloy implanted devices for the digestive tract.

1. Introduction

Magnesium (Mg) and its alloys have gathered much attention as alternatives to permanent medical implants owing to their suitable mechanical properties and biodegradability [1–3]. In recent years, medical magnesium alloys have made great progress in orthopedics and cardiovascular fields [1,4,5]. With the improvement of magnesium alloy processing technology, the preparation of high-performance magnesium wires, plates, and other mini-size materials has been increasingly mature. There has been an up-surge interest in the potential use of Mg alloys for gastrointestinal surgery, such as the biliary stent [6], the hemostatic clip [7], and the anastomotic staple [8–12] and ring [13].

Unlike the body fluid and blood environments, the gastrointestinal environment is more complex. The gastrointestinal tract consists of the stomach, small intestine, and large intestine. There are some obvious differences between their internal environments due to their different roles in the digestive process [14,15], including pH value, digestive enzymes, and ion concentration (Fig. 1). In the stomach, the range of pH is from 1 to 3, and gastric juice mainly contains stomach acid (hydrochloric acid), Cl^-, and pepsin [16–18]. Lower pH associating with the relevant amount of Cl^- is helpful to break down food and activate pepsinogen but detrimental to the degradation of Mg alloys by affecting the precipitation of magnesium hydroxide on the surface [16,19]. In the small intestine, the range of pH is approximately 5.0–7.7, and intestinal juice contains much pancreatin and buffer solution which can neutralize gastric acid for protecting intestinal mucosa from strong acid attack [14,

Peer review under responsibility of KeAi Communications Co., Ltd.
* Corresponding author. School of Materials Science and Engineering, Southeast University, Jiangning, Nanjing 211189, Jiangsu, China.
E-mail address: baijing@seu.edu.cn (J. Bai).
[1] Yue Zhang and Jian Cao have contributed equally to the work.

https://doi.org/10.1016/j.bioactmat.2021.05.047
Received 31 October 2020; Received in revised form 27 April 2021; Accepted 26 May 2021
Available online 12 June 2021

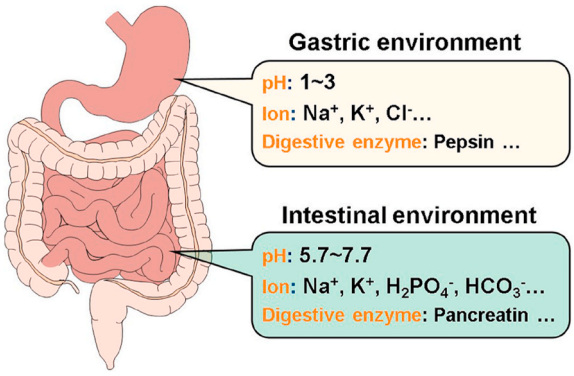

Fig. 1. The diagram of the gastric and intestinal environment.

20,21]. To date, even though numerous efforts based on the actual physiological environments of certain implantation sites have been devoted to evaluating the in vitro corrosion behavior of Mg [6,23–25], reports regarding the degradation of Mg alloys in gastric and intestinal fluids are relatively limited.

As an ongoing exploration, it is well recognized those inorganic species govern the degradation behavior of Mg alloys in biological conditions to a great degree [26–28], and the influence of ion concentration associated with pH value on the degradation behavior of Mg alloys has also been studied extensively [18,28]. In recent years, some studies have found organic compounds, such as serum proteins and several typical amino acids, also have a nonignorable effect on the degradation of Mg alloys by chelating/binding effect or adsorbing on the surface [1,22,29–33]. The adsorbed albumin can serve as an effective protective layer for the degradation of Mg alloys, on the other hand, affect the formation of the degradation layer during immersion, causing a higher corrosion rate by the chelation effect [34]. Additionally, the organics also show different influences on the degradation rate in different media [30]. The addition of glutamic acid postponed the degradation of Mg in phosphate buffer solution (PBS) [35], while it accelerates the degradation rate in Hank's balanced salt solution (HBSS) [36]. Although some studies have investigated the application potential of Mg alloy in the digestive tract, most simulated gastric and intestinal fluid in vitro does not contain enzymes [8,9,12]. Therefore, the effect of pepsin and pancreatin on the degradation of Mg alloys in gastric and intestinal fluids has been unknown.

In this study, the Mg-2Zn wire with a diameter of 1.0 mm was used to resemble as closely as possible the material condition of anastomosis devices, because wires are the raw material for making gastrointestinal anastomosis staples. The effects of two typical digestive enzymes on the degradation of Mg wires were explored to unveil their contribution to the degradation behavior of Mg in simulated gastric and intestinal fluids. Considering the fact that organics has double effects on solution pH derived from their inherent nature of many generic amino acid units with amine (-NH_2) and carboxyl (-COOH) functional terminals thereby influencing the degradation of Mg [35], the pH of solutions was maintained as stable as possible in the immersion test.

2. Materials and methods

2.1. Materials and preparation

Mg-2Zn (wt.%, the chemical composition is shown in Table 1) wires, developed by our research group [37–39] and produced by Suzhou Jingjun New Materials Technology Co. Ltd. China, with a diameter of 1.0 mm were used in this study. The experimental specimens were first ultrasonically cleaned for 5 min in acetone, then polished in a solution consisting of 1 ml nitric acid, 1 ml hydrogen peroxide, and 100 ml distilled water for 1 min. Finally, they were cleaned for 5 min in ethanol ultrasonically and dried under the excitation of UV light in the biosafety cabinet. The surface morphology and microstructure of the wire were observed by a Sirion200 field emission scanning electron microscope (SEM, FEI, Japan) with an acceleration voltage of 20 kV and spot size of 4, and optical metallographic microscopy (BX60 M, Olympus, Japan) as shown in Fig. S1, from which it is clear that original wire surface is smooth and uniform. For preparing the various solutions, hydrochloric acid, sodium hydroxide, potassium dihydrogen phosphate, pepsin, and pancreatin were purchased from Sinopharm Chemical Reagent Co., Ltd. China.

2.2. Immersion test

The degradation behavior was characterized by immersion tests in simulated fluids prepared according to 2015 Chinese pharmacopeia. The simulated gastric fluid (SGF) was obtained by dissolving 1% w/v porcine pepsin in prepared dilute hydrochloric acid solution with pH adjusted to 2.5, and simulated intestinal fluid (SIF) was obtained by dissolving 1% w/v porcine pancreatin in a solution containing 6.804 g L^{-1} KH_2PO_4 with the pH value of 6.8. The pH of solutions was adjusted by the addition of HCl (0.1 mol L^{-1}) and NaOH (0.2 mol L^{-1}), and enzyme-free solutions were used as a control group (Table S1).

Afterward, a static immersion test was carried out in a water bath incubator at (37.5 ± 0.5) °C for 96 h. Wires were cut into 5 cm and hanged into solutions with a ratio of the 1 cm^2 in specimen area to 100 ml in solution volume. The immersion media were replaced at 6 h intervals to minimize the influence of pH change and guarantee the stability of enzymes, and new sterile containers were also replaced at this time. After immersion, samples were taken out of solutions, gently rinsed with distilled water and dried in the air. The degradation products were removed with boiling chromic acid solution containing 180 g L^{-1} chromium oxide in distilled water for 3 min, then rinsed with distilled water and 100% ethanol. After drying, the mass of the samples was determined, and corrosion rate (CR, mm/year) was calculated using the following Eq. (1):

$$CR = 8.76 \times 10^4 \frac{M}{A \cdot t \cdot \rho} \quad (1)$$

where M is the mass loss (g), A is the sample area exposed to the solution (cm^2), t is the immersion time (h) and ρ is the material density (g/cm^3).

2.3. Electrochemical measurements

Potentiodynamic polarization measurements (PDP), electrochemical impedance measurements (EIS) and linear polarization measurements (LPM) of samples were conducted in an electrochemical workstation (PARSTAT 3000A, AMETEK, USA) with a typical three-electrode cell, in which a saturated calomel electrode (SCE) as a reference electrode, a platinum slice as a counter electrode, and the sample as a working electrode. The length of each sample was 5 cm, and the exposed segment in the electrolyte was 4 cm. Samples were clamped by an electrode holder to hang vertically with the same ratio as the immersion test. Before test, samples were immersed in solutions for 5 h till open circuit

Table 1
Chemical composition of Mg-2Zn.

Composition (wt.%)	Zn	Ca	Al	Mn	Si	Cu	Fe	Ni	Mg
Mg-2Zn	2.3033	0.0032	0.0407	0.0250	0.0289	0.0008	0.0079	0.0024	Bal

potential (OCP) reached a relatively stable value. All electrochemical experiments were carried out using a quartz cell at (37.5 ± 0.5) °C, in the atmosphere (mainly 21% O_2, 0.03% CO_2). The anodic and cathodic polarization curves of the samples were measured from the OCP to the anodic and cathodic side with a scan rate of 2 mV s^{-1}, respectively. EIS measurements were performed at the frequency from 100 kHz to 1.0 Hz at OCP with an AC amplitude of 10 mV. The LPM of the samples was measured at ± 20 mV vs. E_{OCP} with a potential sweep rate of 0.16 mV s^{-1}.

2.4. Degradation products analysis

The degradation products on the surface of wires were collected and tested using X-ray diffraction (XRD, Bruker, D8-discover) employing a Cu Kα (λ = 1.54056 Å) radiation source with the voltage of 40 kV and the current of 30 mA. The intensity was collected in the range of 10–90° at a glancing angle of 0.02° and the scanning speed was 0.15 s/step. Fourier transformed infrared (FTIR, Nicolet iS10, USA) was used to record the absorbance spectra of degradation products formed on the Mg surface from different media. The spectra were recorded with a resolution of 0.5 cm^{-1}, taking 512 scans. The chemical composition of surface and cross profile was detected by energy dispersive spectroscopy (EDS, Oxford, UK). XPS measurements were performed to further analyze the surface chemical composition at room temperature with monochromatic Al Kα radiation (1486.6 eV) by X-ray photoelectron spectroscopy (XPS, Phi Quantera II, USA). The survey spectra were collected using a pass energy of 200 eV with 1 eV resolution, and high-energy photoemission spectra were collected using a pass energy of 50 eV with 0.1 eV resolution. Curve fittings were determined using a Gaussian Lorentzian function and a Shirley-type background and performed using the Xpspeak 4.1 software.

3. Results

3.1. Immersion test

The mass loss experiment was employed to monitor the periodical degradation rate of Mg-2Zn wires for 96 h with replacing the immersion fluid every 6 h. Fig. 2(a) depicts the curves of the mass loss ratio in four solutions. The mass loss ratio in SGF is always lower than that in SGF without pepsin, and the gap is getting much wider after immersion for 30 h. In contrast, the presence of pancreatin in SIF results in a higher mass loss ratio in comparison with SIF without pancreatin during the whole immersion process. The corresponding corrosion rate was calculated based on mass loss data and was shown in Fig. 2(b). Samples possess a high corrosion rate at the initial stage of the immersion test, and the rate drops with time in all solutions, which is indicative of the formation of a corrosion product layer on the surface of wires. Nevertheless, the corrosion rate of the sample in SGF without pepsin increases sharply after 18 h of immersion, attributing to the combined effect of Cl^- and the amount of H^+ on the corrosion product. By contrast, the corrosion rate in SGF remains stable. Fig. 2(c) records the variation of pH value. The pH value in solutions without enzymes is higher than that in SGF and SIF. The maximum change of pH occurs at 90 h of immersion with an increment of about 0.37 in SGF without pepsin. As for SIF, although the corrosion rate is the fastest among the four solutions, there is a relatively stable pH value with an increment of less than 0.1.

3.2. Electrochemical characterization

Fig. 3(a) shows the anodic and cathodic PDP curves of the Mg-2Zn wires in different solutions, and the relative electrochemical corrosion parameters determined by the PDP and LPM are listed in Fig. 3(b). The corrosion current density (i_{corr}) is a kinetic parameter to evaluate the

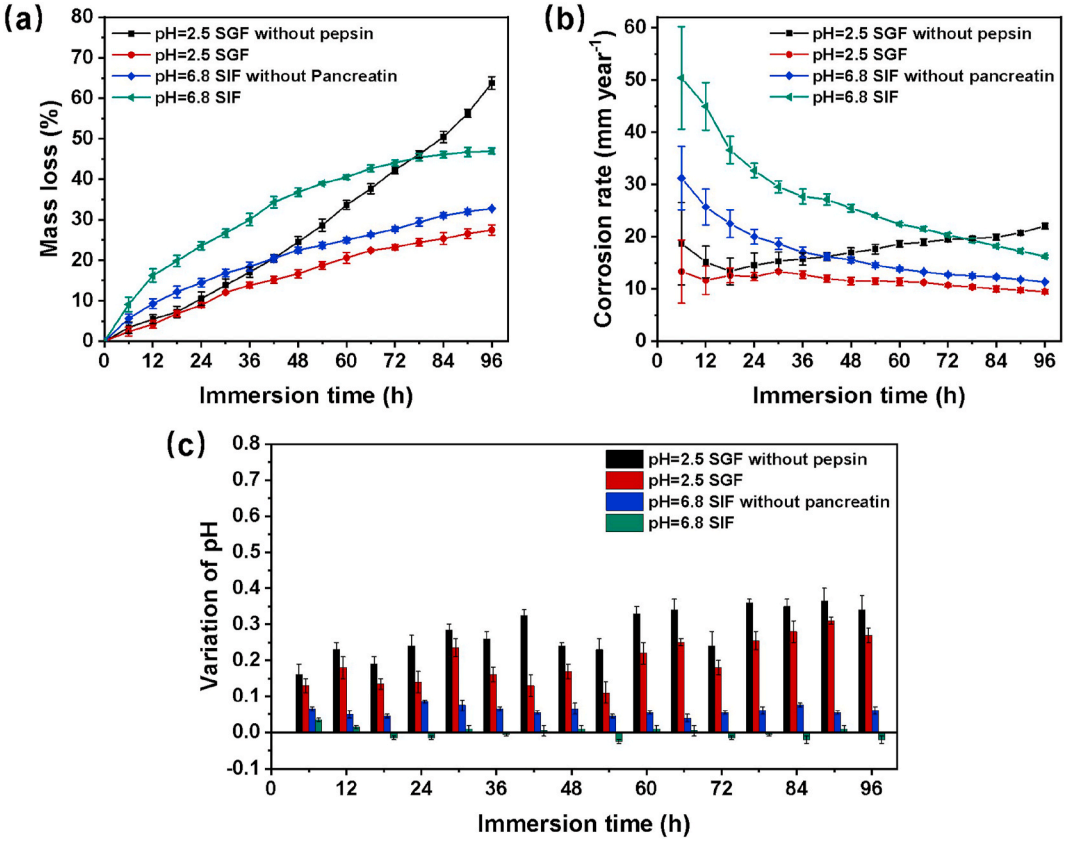

Fig. 2. Plots of the mass loss ratio (a) and corrosion rate(b) calculated from mass loss data of Mg-2Zn wires for 96 h immersion in different media, and variations of pH in solutions (c).

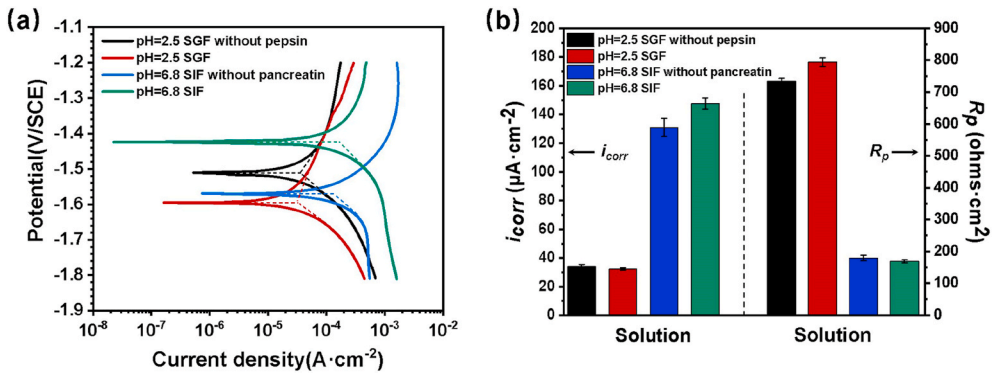

Fig. 3. Typical PDP curves of samples immersed in different solutions (a), and the relative electrochemical corrosion parameters determined by PDP and LPM (b).

corrosion rate, and the polarization resistance (R_p) can profile the corrosion resistance [40,41]. The i_{corr} decreases slightly when the Mg-2Zn wire is immersed in SGF, while the sample immersed in SIF has higher i_{corr} than that of SIF without pancreatin. Besides, samples immersed in SGF and SIF without pancreatin have higher R_p than that of SGF without pepsin and SIF, exhibiting a low tendency toward corrosion and better corrosion resistance.

Fig. 4 shows the EIS results of Mg wires immersed in four solutions. The Nyquist diagram (Fig. 4(a)) contains a low-frequency capacitive reactance arc and high-frequency capacitive reactance arc, corresponding to two time constants displayed in the Bode plots of -phase angle vs frequency (Fig. 4(b)). A slight disturbance occurred at the high frequency, which might originate from surface bubbles generated during the static immersion before the measurement. Generally, a larger capacitive loop represents a better corrosion resistance [42], which is corresponded to a larger low-frequency modulus impedance ($|Z|_{1.0Hz}$). Thus, the $|Z|_{1.0Hz}$ value obtained from Nyquist curves can be arranged in the following order, SGF > SGF without pepsin, and SIF without pancreatin > SIF, indicating the pepsin to a certain extent weakens the corrosion rate and the pancreatin accelerates the corrosion rate. These findings are consistent with the results of the mass loss test.

3.3. Surface morphology

SEM morphologies of the samples after immersion in solutions for 24 h and 96 h are displayed in Fig. 5. The related results of EDS analysis are shown in Fig. 6. For the sample immersed in SGF without pepsin after 24 h, there are numerous cracks on the surface, disclosing a honeycomb film at the black area (Fig. 5(a)). EDS results signified the predominant constituents are O and Mg. As a comparison, a dense degradation product with numerous micro-cracks spanning the whole of the surface is observed on the sample soaked in SGF (Fig. 5(b)). The element P and N is detected on the surface, indicating the pepsin participates the formation of degradation products. In the case of the sample in SIF without pancreatin, there are many bright fragments as shown in Fig. 5(c), and their composition is comprised of Mg, O, and P. For the sample in SIF, the bright pieces become thicker than that in SIF without pancreatin. Many flocculent deposits containing element N partially distribute at random on the surface. The severe non-uniform corrosion is not observed at this time on all samples' surfaces, while the corrosion morphology has been significantly different (Fig. 5(a1) to (d1)).

With prolonging the immersion time to 96 h, the surface of the sample in SGF without pepsin is completely covered with white degradation products (Fig. 5(e)), while the severe localized corrosion can be seen in Fig. 5(e1). As for the sample in SGF, the area of uniform corrosion is larger, while the localized corrosion is still inevitable. EDS analysis demonstrates the element N content of area H is higher than that of area I, indicating more pepsin exist in the degradation product at the uniform corrosion area. For the sample in SIF without pancreatin, the degradation product is fragile and easy to fall off. The surface is very uniform after the removal of the degradation products in Fig. 5(g1). However, Fig. 5(h1) shows a comparison of the sample surfaces after immersed in SIF. The amount of N element is detected on the area K and L (Fig. 5(h)), suggesting the presence of pancreatin.

3.4. The composition of degradation products

Fig. 7(a) shows XRD patterns of the samples after 48 h immersion. The result of the sample immersed in SGF without pepsin demonstrates the presence of magnesium hydroxide ($Mg(OH)_2$, reference PDF card No. 44-1482), suggesting that the $Mg(OH)_2$ can be formed on the surface of Mg in solution with a pH value of 2.5. The peaks of samples in SIF and SIF without pancreatin are designated magnesium hydrogen phosphate ($MgHPO_4{\cdot}3H_2O$, reference PDF card No. 35-0780). Previous studies have also shown that the $MgHPO_4{\cdot}3H_2O$ can be formed in a phosphate buffer solution with a constant pH of 6.8 [43]. However, due to the relatively thin and fragile corrosion layer, the magnesium hydroxide cannot be detected and the result of magnesium hydrogen phosphate in SIF without pancreatin is not obvious.

To give an insight into the composition of the products layer, FTIR

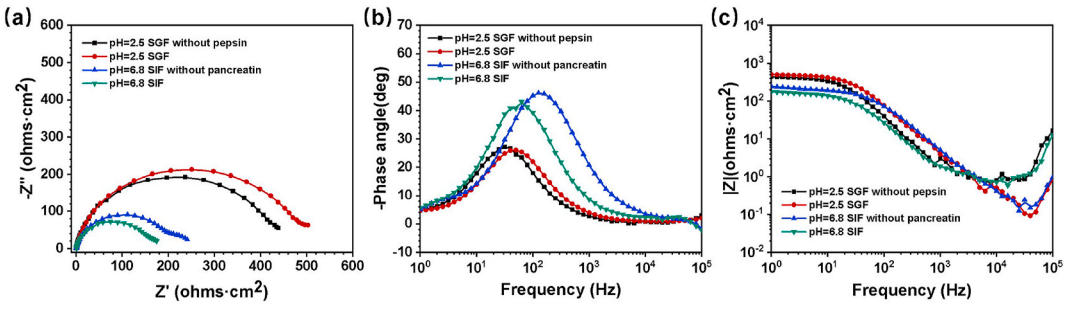

Fig. 4. Plots of EIS results of Mg-2Zn wires immersed in different media, (a) Nyquist, (b) Bode plots of -phase angle vs frequency, (c) Bode plots of |Z| vs frequency (In order to compare the difference among samples in solutions, the solution resistance was zeroed).

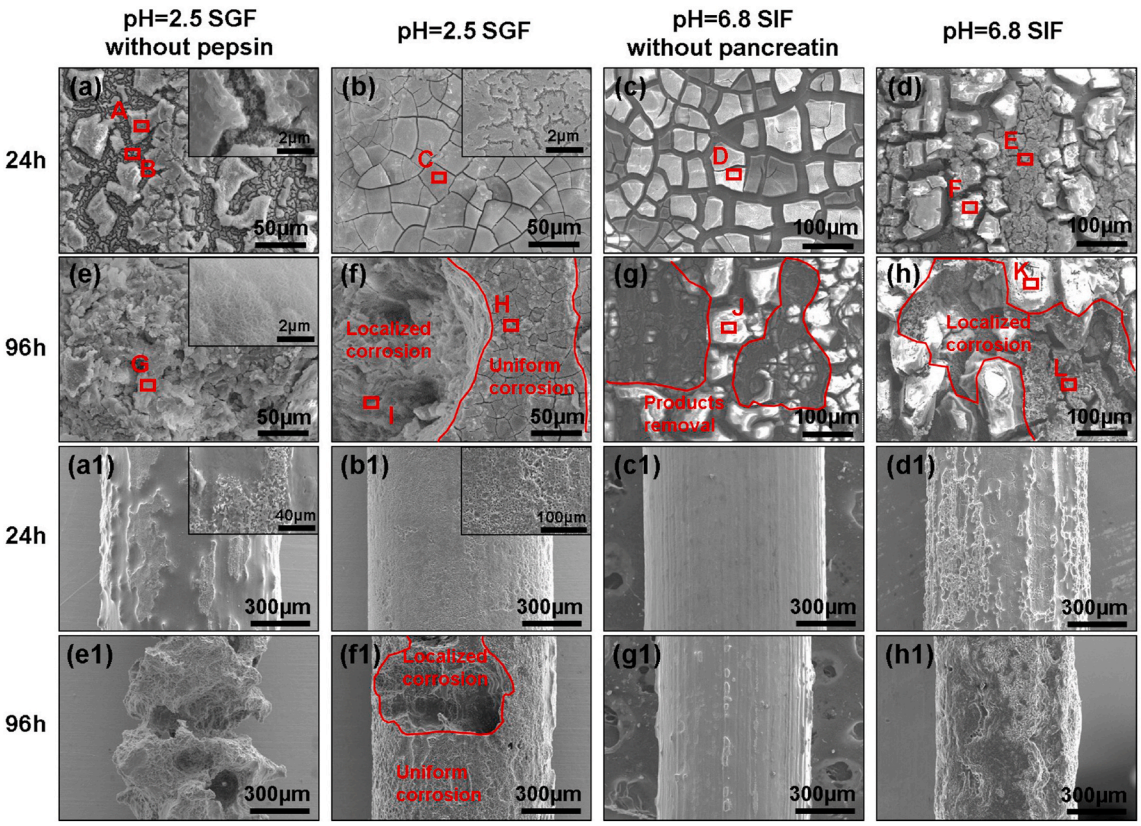

Fig. 5. SEM images of degraded surfaces after immersion of 24 h, (a) SGF without pepsin, (b) SGF, (c) SIF without pancreatin, (d) SIF, and of 96 h (e) SGF without pepsin, (f) SGF, (g) SIF without pancreatin, (h) SIF. (a1-h1) are the macro morphologies of samples corresponding to (a–h) after removing the degradation products. Area A-L were selected for EDS analysis.

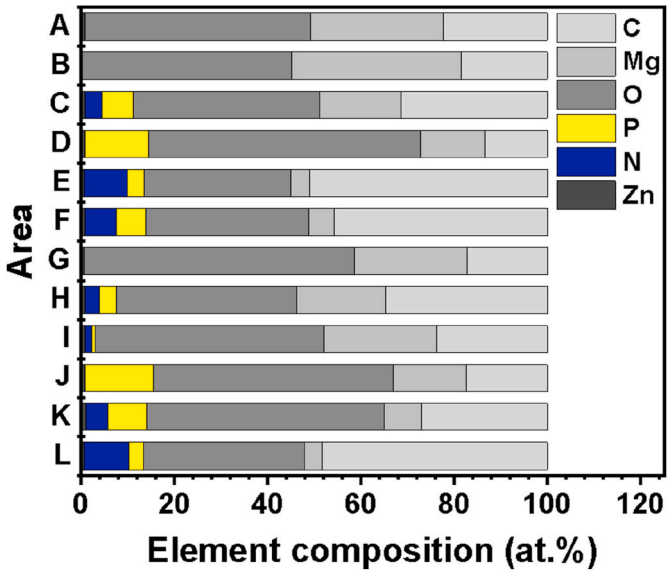

Fig. 6. Elemental composition of the selected areas marked in SEM images.

reflection spectra were collected from samples. As shown in Fig. 7(b), an absorption band at 3698 cm^{-1} corresponds to the Mg-OH stretching vibration, indicating the formation of Mg $(OH)_2$ on the surface of samples in the SGF and SGF without pepsin. The broadband centered near 3500 cm^{-1} is attributed to the stretching vibration of the O-H group [44]. Peaks at 2922 and 2855 cm^{-1} are attributed to stretching vibrations of C–H groups, and a band at approximately 1648 cm^{-1} could be ascribed to the bending vibration of carbonyl (C=O) in association state resulting from the enzymes [33,35]. The shoulder at 1640 cm^{-1} is ascribed to an OH-bending mode of water and/or amide of organic molecules. There may be some hidden peaks at 1600–1650 cm^{-1} on behalf of C=N or C=C [24,36,45], suggesting small amounts of the enzyme involved in the formation products layer. Strong IR signals in the range 1290–1550 cm^{-1} arise from the anti-symmetrical CO_3^{2-} stretching and/or amide of organic components from pepsin [36,46,47]. Additionally, the bands at the range of 850–1295 cm^{-1} could be designated to bending vibration of CO_3^{2-} or P-O, such as HPO_4^{2-}, or organics.

XPS measurements were conducted to obtain more detailed information regarding the influence of organic species on the chemical composition of degradation product layers. Fig. 8(a) specifies the entire range of binding energy measurements of samples immersed in SGF and SIF. The results show that the degradation products on the surface of samples are mainly composed of C, N, P, Mg, and O elements. Tabulated XPS data are used to investigate the peak position related to C, N and their compounds on the XPS spectra (Table 2). Concerning C 1s spectra, the peak is composed of five contributions at 284.6 eV, 285.4 eV, 286.2 eV, 287.1 and 288.3 eV (Fig. 8(b) and (e)), which represents the carbon bonds C-H/C-C, C-N, C-O, C=N, and O=C-N, respectively. In general, the peak at 286.2 eV is assigned to NH-CHR-CO carbons of the protein backbone, and the peak at 288.3 eV is assigned to the -CO-NH- peptide bonds of proteins. Moreover, the deconvolution of N 1 s spectra (Fig. 8 (c) and (d)) reveals two components, centered at 399.4 eV and 400.0 eV, corresponding to the C–N and C=O-NH bonds, as expected for the amine or amide groups of enzymes. The presence of N can be a reliable criterion for protein adsorption. Thus, these characteristic bands indicate the presence of enzymes on sample surfaces.

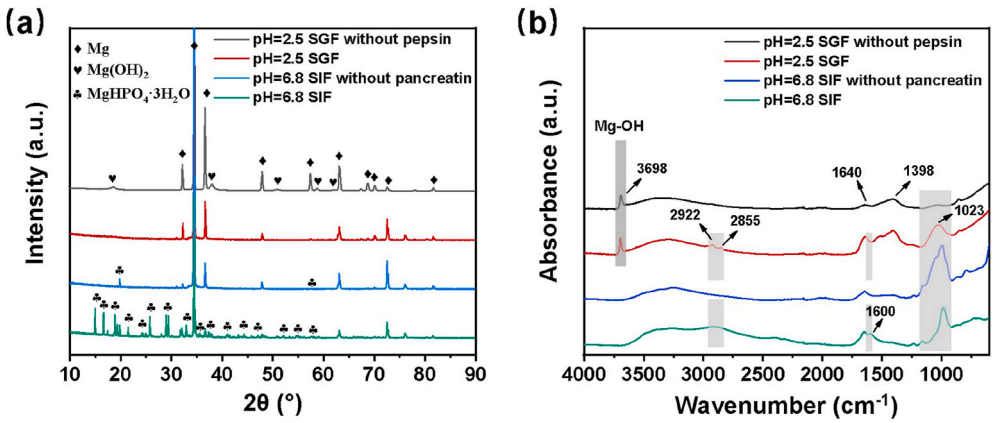

Fig. 7. (a) XRD patterns and (b) FTIR spectra of samples after 48 h immersion in four solutions (Light grey region refers to the bands with differences, Dark grey region refers to the bands from magnesium hydroxide).

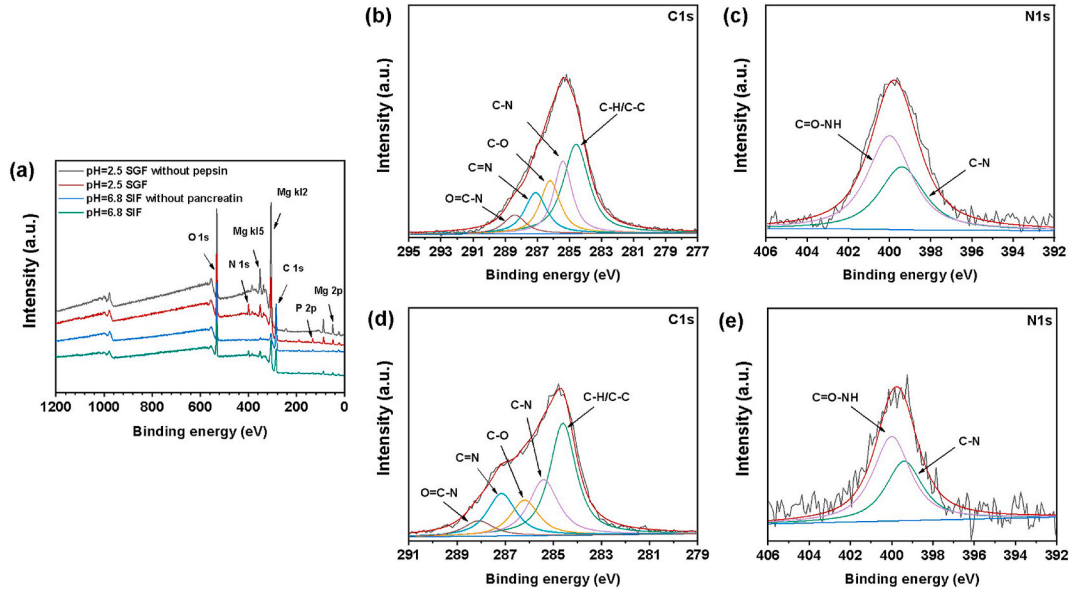

Fig. 8. XPS broad survey of the surface after immersion (a) and high resolution XPS spectra, (b) C1s and (c) N1s of the sample in SGF, (d) C1s and (e) N1s of the sample in SIF.

Table 2
Parameters used for C1s and N1s XPS spectra.

Peak	Species	Binding energy (eV)	Refs
C 1s	C-H/C-C	~284.6	[48,49]
	C-N	~285.4	[48,49]
	C-O	~286.2	[48,49]
	C=N	~287.1	[33,50]
	O=C-N	~288.3	[48,49]
N 1s	C-N	~399.4	[33]
	C=O-NH	~400.0	[33,51–53]

3.5. Chemical element analysis of cross-sections

To validate the variation of the chemical composition in the inner of degradation products, chemical element mapping and linear scanning were conducted for analyzing layer cross-sections. Fig. 9 shows the distributions of the predominant elements C, O, P, and Mg probed from all samples. As expected, the existence of O and Mg in Fig. 9(a) and (c) means the presence of metal oxides. The distribution of C has little fluctuation along with the entire corrosion layer in them, while there is a component transition layer measured from the curves of relative intensities in Fig. 9(b) and (d). Furthermore, more obvious difference from the distributions of P are distinguished as shown in Fig. 9(a) and (b), indicating the organic components distribute in the interface. For samples immersed in SIF and SIF without pancreatin, there is no obvious difference in element distribution due to the presence of hydrogen phosphate ion in the solution. Nevertheless, the fluctuation of P in Fig. 9 (b) and (d) is observed, which may be related to the adsorption of enzymes. Table 3 shows atomic percentages of related elements calculated by selected area analysis. The relative content of C, N, and P is increased distinctively as the enzyme addition.

4. Discussion

In the present work, we studied the effects of pepsin and pancreatin on the degradation behavior of Mg-2Zn alloy wires based on the simulated gastric and intestinal fluids. The results demonstrate that the digestive enzyme plays a particularly important role in affecting the degradation behavior of Mg wires. Similar to albumin, the enzyme is a protein composed of many amino acids joined by peptide bonds. Herein, we summarized existing investigations with regards to the contribution of albumin and amino acids to the degradation performance of Mg alloys

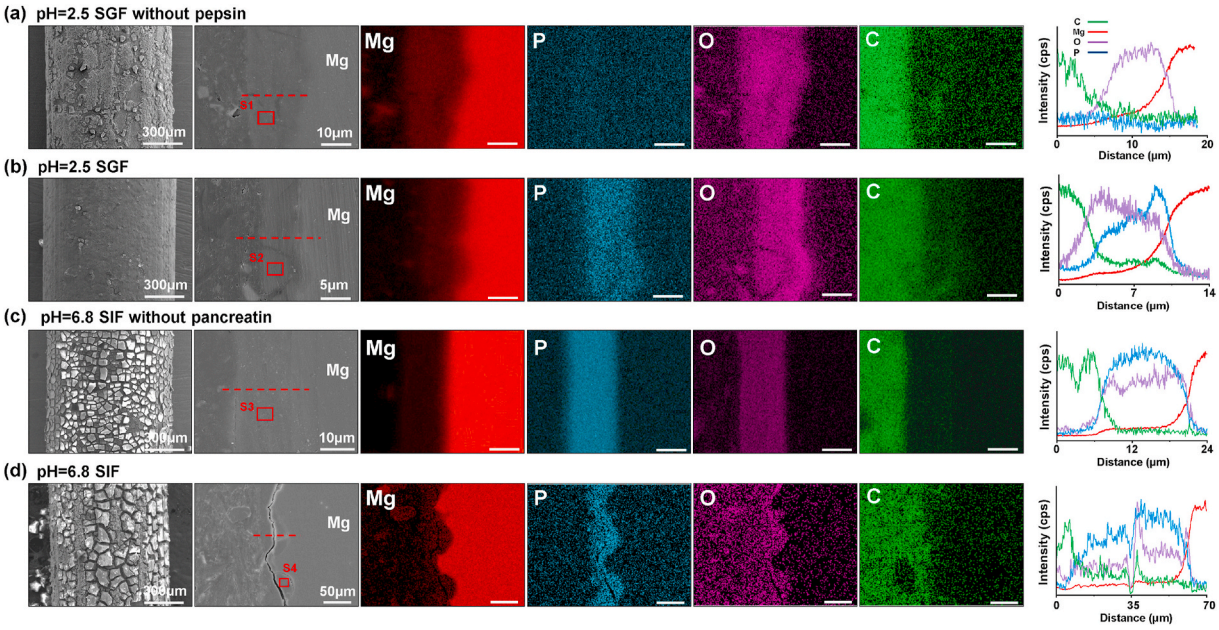

Fig. 9. EDS mapping data and line scanning of degradation products after immersion in solutions for 24 h (the red line refers to the line scanning position).

Table 3
Element composition of selected areas (S1, S2, S3 and S4) marked in cross-sections of products.

Elemental composition (at. %)	S1	S2	S3	S4
C	18.19	40.65	13.54	36.60
Mg	30.09	21.12	14.45	13.58
O	51.31	32.73	57.44	27.92
P	0	2.9	13.64	19.89
N	0	1.71	0	1.06
Zn	0.4	0.89	0.93	0.95

Table 4
Comparison of the influence of the protein and amino acid on degradation rate in different solutions through the immersion test (the interval means the time of solution replacement, ↑ refers to the accelerating effect of organics in medium, ↓ refers to the inhibiting effect of organics in medium, ↑↓ refers to the accelerating effect at first and then the inhibiting effect of organics in medium).

Materials	Solutions	Maximum pH of solution	Interval	Effects	Refs
Pure Mg	PBS +0.032 mg/L alanine	~ 8.93	None	↓	[35] [36]
	PBS + 0.012 mg/L glutamic	~ 8.63	None	↓	[32] [30]
	PBS + 0.03 mg/L lysine	~ 8.52	None	↓	[54] Present work
Pure Mg	HBSS + 292 mg/L L-glutamine	~ 9.05	2–3 days	↑	
	HBSS + 862 mg/L L-alanyl-L-glutamine	~ 8.91	2–3 days	↑	
Mg-1.5Ca	0.9 wt% NaCl + 1 g/L BSA	–	None	↓	
	0.9 wt% NaCl + 10 g/L BSA	–	None	↓	
Pure Mg	0.9 wt% NaCl + 0.1 g/L BSA	~ 10.37	None	↓	
M1A	SBF + 40 g/L BSA	–	None	↑↓	
Mg-2Zn	pH = 2.5 SGF with pepsin	~ 2.78	6 h	↓	
	pH = 6.8 SIF with pancreatin	~ 6.84	6 h	↑	

in different simulated physiological fluids in Table 4. It can be seen the influence of organic components on the degradation of Mg had not reached a consensus.

In general, the proteins are considered to have a chelating and barrier function, which is the key factor affecting the corrosion rate of magnesium alloy [1]. The delayed corrosion was confirmed due to the physical barrier by adsorbing proteins on the metal surface, and the accelerated corrosion was deemed to the effect of the binding to metal cations [1,53–55]. Wang et al. [54] found the blocking effect of the adsorbed protein layer only mattered in the initial degradation stage but increased metal dissolution in the later stage. Xin et al. [55] also found this blocking effect weakened dramatically with elongating the immersion period. In contrast, the bovine serum albumin (BSA) could hinder the corrosion rate of Mg alloys in the NaCl solution [32,56].

As shown in Figs. 2(a) and Fig. 5, the pepsin has an obvious inhibitory effect for the degradation of Mg wires in SGF, impeding the formation of the pitting corrosion. Instead, the addition of the pancreatin in SIF accelerates the degradation rate of wires and leads to uneven corrosion. These two results seem to contradict each other. Nevertheless, the inorganic environment of SGF with the strong acid and abundant Cl^- is different from that of SIF. The chloride ion can cause the breakdown of the magnesium hydrate passive film and lead to localized corrosion [19,28]. A lower pH value is detrimental to the formation of magnesium hydrate since that the solubility is associated with the pH value [26]. Inversely, the passivation film formed by the hydrogen phosphate and Mg ion can decrease the corrosion rate. Therefore, in Fig. 2(b), an acceleration of corrosion rate of the sample in SGF without pepsin occurs after immersion of 18 h, while the corrosion rate of the sample in SIF without pancreatin gradually decreases and then reaches stability. Moreover, there are also reports that the isoelectric point of the protein is the main factor alternating the corrosion rate [35,36]. As depicted in Fig. 2(c), the pH of all solutions is stable in this study.

The adsorption of proteins on the metal surface during the immersion test has been recognized. Divalent cations, such as Ca^{2+} or Mg^{2+}, can serve as bridging agents to enhance the adsorption of albumin molecules through electrostatic interaction [32,57]. It is reported proteins could adsorb on the Mg surface, thereby leading to the variation of the surface layer compactness or thickness, and resulting in a different influence on the corrosion of Mg alloys [58,59]. As shown in Figs. 6–9, N and P elements are detected by EDS in the surface and cross-section of

products, and FTIR and XPS spectra also indicate the existence of organic components in the products' layer. Both enzymes affect the formation of degradation products. Associating the different results in SGF without pepsin and SIF without pancreatin, this opposite effect of enzymes in SGF and SIF may be attributed to the inorganic ionic environment. Therefore, these basic mechanisms are depicted in Fig. 10.

When sample are immersed into SGF without pepsin, magnesium reacts quickly and releases an amount of Mg^{2+} ions, alkaline hydroxyl anions, and hydrogen gas (Formula (1), (2)).

$$Mg(s) \rightarrow Mg^{2+}(aq) + 2e^{-} \text{ (anodic reaction)} \quad (1)$$

$$2H_2O + 2e^{-} \rightarrow H_2(g)\uparrow + 2OH^{-}(aq) \text{ (cathodic reaction)} \quad (2)$$

$$Mg^{2+}(aq) + 2OH^{-}(aq) \rightarrow Mg(OH)_2(s) \text{ (Products formation)} \quad (3)$$

Owing to the rich hydrogen ions in the solution, the surface of wires is relatively homogeneous in the early stages (Fig. 10(a1)). In general, the magnesium hydroxide film is difficult to form in an acidic environment [26,27]. However, a large number of alkaline hydroxyl anions and Mg ions are generated with the dissolution of magnesium, which is in favor of the formation of a diffusion layer with higher pH around the wire's surface [60]. Thus, as shown in Figs. 5 and 9, an uneven protective $Mg(OH)_2$ film layer is formed on the sample surface (Fig. 10(a2)) (Formula (3)).

As the soaking time increases, the surface is completely covered by the corrosion product. Under the combined effects of chlorine ions and hydrogen ions, the surface becomes uneven, and finally, severe localized corrosion occurred (Fig. 10(a3)). When the sample is immersed in SGF, hydrogen evolution and enzymes' adsorption occur simultaneously (Fig. 10(b1)). Due to the pepsin adsorbed on the sample surface, the interface between the sample and solution could be changed, causing the variation of electrochemical parameters [32,61]. As the pepsin added, the $|Z|_{1.0Hz}$ value increases from 446.06 Ω cm^2 to 505.35 Ω cm^2, representing better corrosion resistance of the wire in SGF. The adsorbed pepsin could increase the integrity of the film layer and cover more surface of Mg wires, hindering the corrosion of Cl^{-} (Fig. 5(b)). However, the adsorption of pepsin is not a perfect barrier to prevent corrosion (Fig. 5(f)). The localized corrosion is observed (Fig. 10(b2)) and then extends more (Fig. 10(b3)). For the SIF without pancreatin, $MgHPO_4{\cdot}3H_2O$ film forms on the Mg alloy substrate continually (Fig. 10(c2)). The diffusion zone between the conversion solution and Mg-P film transfers Mg ions and hydrogen gas to the solution and conversely transfers HPO_4^{2-} and H^{+} ions from the solution to the Mg-P film [43]. It is recognized that the hydrogen phosphate is beneficial to decrease the corrosion rate and uniform corrosion of magnesium alloys [26,28]. Nevertheless, the $|Z|_{1.0Hz}$ value decreases with the addition of pancreatin. The corrosion resistance of the sample in SIF is lower than that of the sample in SIF without pancreatin. Besides, the lower R_p value from the LPM result and the immersion test also showed that the addition of the pancreatin increases the corrosion rate. Although the adsorbed pancreatin is involved in the formation of corrosion products, it is less dense than the Mg-P chemical layer, causing easier penetration of the aqueous solution [54]. The adsorption layer of pancreatin affects the formation of magnesium phosphate (Fig. 10(d2)). Hence, the uneven corrosion surface is observed in Fig. 5(d1) and a higher corrosion rate is found.

5. Conclusions

In this study, we investigated the effect of digestive enzymes, pepsin and pancreatin, on the degradation behavior of Mg-2Zn alloy wires based on the simulated gastric and intestinal fluids. The in vitro immersion experiments and electrochemical corrosion measurements indicated that the degradation rate of Mg wire declined with the addition of pepsin in SGF but rose with the addition of pancreatin in SIF. Completely different degradation morphologies were depicted by SEM. Moreover, EDS, FTIR and XPS results demonstrated that both the pepsin and pancreatin participated the formation of the degradation product layer. The physical barrier effect of pepsin adsorption retarded the

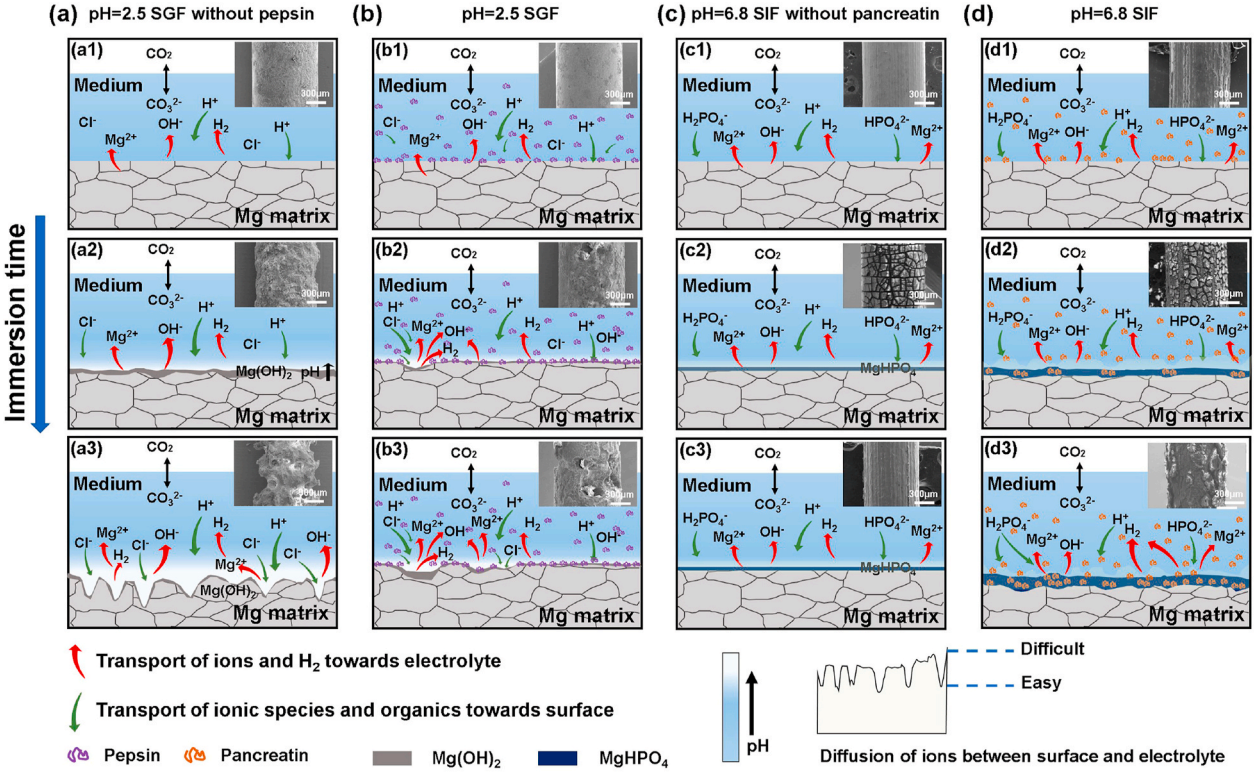

Fig. 10. Schematic illustration of Mg-2Zn wires degradation in different media as the immersion time increases, (a) degradation in SGF without pepsin, (b) degradation in SGF, (c) degradation in SIF without pancreatin, (d) degradation in SIF (the number 1 to 3 means the increase of immersion time).

pitting corrosion and corrosion rate in SGF, but it is not a perfect barrier to prevent corrosion. The localized corrosion is observed after the immersion of 96 h in SGF. Instead, the adsorption of pancreatin affected the integrity of magnesium hydrogen phosphate film, causing the degraded surface uneven. The research findings indicated that the effect of enzymes on the degradation of Mg should be studied based on their living environment, and more investigations regarding the influence of organic components are still needed to be further explored.

CRediT authorship contribution statement

Yue Zhang: Conceptualization, Methodology, Writing – original draft. **Jian Cao:** Data curation, Methodology. **Xianli Wang:** Data curation, Investigation. **Huan Liu:** Investigation, Formal analysis. **Yi Shao:** Investigation. **Chenglin Chu:** Resources, Methodology. **Feng Xue:** Conceptualization, Funding acquisition. **Jing Bai:** Conceptualization, Visualization, Writing – review & editing.

Acknowledgement

This work was supported by the National Key Research and Development Program of China (2016YFC1102402), the National Natural Science Foundation of China (51971062), the Science and Technology Project of Jiangsu Province (BE2019679), the Technological Innovation of key Industry of Suzhou (SYG201904), and the open research fund of Jiangsu Key Laboratory for Advanced Metallic Materials (AMM2021A01).

Appendix A. Supplementary data

Supplementary data to this article can be found online at https://doi.org/10.1016/j.bioactmat.2021.05.047.

Declaration of competing interest

The authors declare no conflict of interest.

References

[1] Y.F. Zheng, X.N. Gu, F. Witte, Biodegradable metals, Mat. Sci. Eng. Res. 77 (2014) 1–34, https://doi.org/10.1016/j.mser.2014.01.001.
[2] G.L. Song, S. Song, A possible biodegradable magnesium implant material, Adv. Eng. Mater. 9 (2010) 298–302, https://doi.org/10.1002/adem.200600252.
[3] Y. Sun, H. Wu, W. Wang, R. Zan, H. Peng, S. Zhang, X. Zhang, Translational status of biomedical Mg devices in China, Bioact. Mater. 4 (2019) 358–365, https://doi.org/10.1016/j.bioactmat.2019.11.001.
[4] J. Zhang, H.Y. Li, W. Wang, H. Huang, J. Pei, H.Y. Qu, G.Y. Yuan, Y.D. Li, The degradation and transport mechanism of a Mg-Nd-Zn-Zr stent in rabbit common carotid artery: a 20-month study, Acta Biomater. 69 (2018) 372–384, https://doi.org/10.1016/j.actbio.2018.01.018.
[5] A. Chaya, S. Yoshizawa, K. Verdelis, N. Myers, J. Costello B, D. Chou, S. Pal, S. Maiti, N. Kumta P, C. Sfeir, In vivo study of magnesium plate and screw degradation and bone fracture healing, Acta Biomater. 18 (2015) 262–269, https://doi.org/10.1016/j.actbio.2015.02.010.
[6] Y. Zhang, K.Y. Chen, H. Liu, Y. Shao, C.L. Chu, F. Xue, J. Bai, A study of a biodegradable braided Mg stent for biliary reconstruction, J. Mater. Sci. 55 (2020) 17170–17182, https://doi.org/10.1007/s10853-020-05289-9.
[7] X. Yu, D.Y. Li, Y.C. Liu, P.F. Ding, X.H. He, Y. Zhao, M.F. Chen, D.B. Liu, In vitro and in vivo studies on the degradation and biosafety of Mg-Zn-Ca-Y alloy hemostatic clip with the carotid artery of SD rat model, Mat. Sci. Eng. C Mater. 115 (2020) 111093, https://doi.org/10.1016/j.msec.2020.111093.
[8] M. Gao, D. Na, X.Q. Ni, L.H. Song, I.P. Etim, K. Yang, L.L. Tan, Z. Ma, The mechanical property and corrosion resistance of Mg-Zn-Nd alloy fine wires in vitro and in vivo, Bioact. Mater. 6 (2021) 55–63, https://doi.org/10.1016/j.bioactmat.2020.07.011.
[9] H.L. Wu, C.L. Zhao, J.H. Ni, S.X. Zhang, J.Y. Liu, J. Yan, Y.G. Chen, X.N. Zhang, Research of a novel biodegradable surgical staple made of high purity magnesium, Bioact. Mater. 1 (2016) 122–126, https://doi.org/10.1016/j.bioactmat.2016.09.005.
[10] H. Amano, K. Hanada, A. Hinoki, T. Tainaka, C. Shirota, W. Sumida, K. Yokota, N. Murase, K. Oshima, K. Chiba, Y. Tanaka, H. Uchida, Biodegradable surgical staple composed of magnesium alloy, Sci. Rep. UK 9 (2019) 1–8, https://doi.org/10.1038/s41598-019-51123-x.
[11] J. Xia, H. Chen, J. Yan, H.L. Wu, H. Wang, J. Guo, X.N. Zhang, S.X. Zhang, C. L. Zhao, Y.G. Chen, High-Purity magnesium staples suppress inflammatory response in rectal anastomoses, ACS Appl. Mater. Int. 9 (2017) 9506–9515, https://doi.org/10.1021/acsami.7b00813.
[12] S. Qu, J.Z. Xia, J. Yan, H.L. Wu, H. Wang, Y. Yi, X.N. Zhang, S.X. Zhang, C.L. Zhao, Y.G. Chen, In vivo and in vitro assessment of the biocompatibility and degradation of high-purity Mg anastomotic staples, J. Biomater. Appl. 31 (2017) 1203–1214, https://doi.org/10.1177/0885328217692948.
[13] Q.L. Huang, L. Liu, H. Wu, K.M. Li, N.F. Li, Y. Liu, The design, development, and in vivo performance of intestinal anastomosis ring fabricated by magnesium-zinc-strontium alloy, Mat. Sci. Eng. C Mater. 106 (2020) 110158, https://doi.org/10.1016/j.msec.2019.110158.
[14] J. Fallingborg, Intraluminal pH of the human gastrointestinal tract, Dan. Med. Bull. 46 (1999) 183–196.
[15] R.S. Jadcherla, C. Berseth, Chapter 3-development of gastrointestinal motility reflexes, in: J. Neu (Ed.), Gastroenterology and Nutrition: Neonatology Questions and Controversies, Elsevier Inc., 2012, pp. 27–37, https://doi.org/10.1016/B978-1-4377-2603-9.00003-X.
[16] R.L. Wilson, C.E. Stevenson, Chapter 56 - anatomy and physiology of the stomach, in: C.J. YEO (Ed.), Shackelford's Surgery of the Alimentary Tract, Elsevier Inc. Philadelphia, 2019, pp. 634–646, https://doi.org/10.1016/B978-0-323-40232-3.00056-X.
[17] M. Vertzoni, E. Pastelli, D. Psachoulias, L. Kalantzi, C. Reppas, Estimation of intragastric solubility of drugs: in what medium? Pharm. Res. Dordr. 24 (2007) 909–917, https://doi.org/10.1007/s11095-006-9209-9.
[18] C. Tedeschi, V. Clement, M. Rouvet, B. Valles-Pamiesc, Dissolution tests as a tool for predicting bioaccessibility of nutrients during digestion, Food Hydrocolloid 23 (2009) 1228–1235, https://doi.org/10.1016/j.foodhyd.2008.09.012.
[19] M.C. Zhao, M. Liu, G.L. Song, A. Atrens, Influence of pH and chloride ion concentration on the corrosion of Mg alloy ZE41, Corros. Sci. 50 (2008) 3168–3178, https://doi.org/10.1016/j.corsci.2008.08.023.
[20] M. Falavigna, M. Klitgaard, E. Steene, G.E. Flaten, Mimicking regional and fasted/fed state conditions in the intestine with the mucus-PVPA in vitro model: the impact of pH and simulated intestinal fluids on drug permeability, Eur. J. Pharm. Sci. 132 (2019) 44–54, https://doi.org/10.1016/j.ejps.2019.02.035.
[21] T. Di, G.J. Chen, Y. Sun, S.Y. Qu, X.X. Zeng, H. Ye, In vitro digestion by saliva, simulated gastric and small intestinal juices and fermentation by human fecal microbiota of sulfated polysaccharides from Gracilaria rubra, J. Funct. Foods 40 (2018) 18–27. Error! Hyperlink reference not valid.
[22] A. Yamamoto, S. Hiromoto, Effect of inorganic salts, amino acids and proteins on the degradation of pure magnesium in vitro, Mat. Sci. Eng. C Mater. 29 (2009) 1559–1568, https://doi.org/10.1016/j.msec.2008.12.015.
[23] L. Mao, G.Y. Yuan, S.H. Wang, J.L. Niu, G.H. Wu, W.J. Ding, A novel biodegradable Mg-Nd-Zn-Zr alloy with uniform corrosion behavior in artificial plasma, Mater. Lett. 88 (2012) 1–4, https://doi.org/10.1016/j.matlet.2012.08.012.
[24] R.C. Zeng, X.T. Li, L.J. Liu, S.Q. Li, F. Zhang, In vitro degradation of pure Mg for esophageal stent in artificial saliva, J. Mater. Sci. Technol. 32 (2016) 437–444, https://doi.org/10.1016/j.jmst.2016.02.007.
[25] S.Y. Zhang, Y.Z. Bi, J.Y. Li, Z.G. Wang, J.M. Yan, J.W. Song, H.B. Sheng, H.P. Guo, Y. Li, Biodegradation behavior of magnesium and ZK60 alloy in artificial urine and rat models, Bioact. Mater. 2 (2017) 53–62, https://doi.org/10.1016/j.bioactmat.2017.03.004.
[26] R.C. Zeng, Y. Hu, S.K. Guan, H.Z. Gui, E.H. Han, Corrosion of magnesium alloy AZ31: the influence of bicarbonate, sulphate, hydrogen phosphate and dihydrogen phosphate ions in saline solution, Corros. Sci. 86 (2014) 171–182, https://doi.org/10.1016/j.corsci.2014.05.006.
[27] L. Wang, T. Shinohara, B.P. Zhang, Influence of chloride, sulfate and bicarbonate anions on the corrosion behavior of AZ31 magnesium alloy, J. Alloy Compd. 496 (2010) 500–507, https://doi.org/10.1016/j.jallcom.2010.02.088.
[28] Y. Jang, B. Collins, J. Sankar, Y. Yun, Effect of biologically relevant ions on the corrosion products formed on alloy AZ31B: an improved understanding of magnesium corrosion, Acta Biomater. 9 (2013) 8761–8770, https://doi.org/10.1016/j.actbio.2013.03.026.
[29] H. Medhashree, A.N. Shetty, Electrochemical investigation on the effects of sulfate ion concentration, temperature and medium pH on the corrosion behavior of Mg–Al–Zn–Mn alloy in aqueous ethylene glycol, J. Magnes. Alloy 5 (2017) 64–73, https://doi.org/10.1016/j.jma.2016.12.003.
[30] W. Yan, Y.J. Lian, Z.Y. Zhang, M.Q. Zeng, Z.Q. Zhang, Z.Z. Yin, L.Y. Gui, R.C. Zeng, In vitro degradation of pure magnesium–the synergetic influences of glucose and albumin, Bioact. Mater. 5 (2020) 318–333, https://doi.org/10.1016/j.bioactmat.2020.02.015.
[31] Z.Q. Zhang, L. Wang, M.Q. Zeng, R.C. Zeng, M.B. Kannan, C.G. Lin, Y.F. Zheng, Biodegradation behavior of micro-arc oxidation coating on magnesium alloy-from a protein perspective, Bioact. Mater. 5 (2020) 398–409, https://doi.org/10.1016/j.bioactmat.2020.03.005.
[32] C.L. Liu, Y.J. Wang, R.C. Zeng, X.M. Zhang, W.J. Huang, P.K. Chu, In vitro corrosion degradation behaviour of Mg–Ca alloy in the presence of albumin, Corros. Sci. 52 (2010) 3341–3347, https://doi.org/10.1016/j.corsci.2010.06.003.
[33] L.J. Liu, Y. Meng, A.A. Volinsky, H.J. Zhang, L.N. Wang, Influences of albumin on in vitro corrosion of pure Zn in artificial plasma, Corros. Sci. 153 (2019) 341–356, https://doi.org/10.1016/j.corsci.2019.04.003.
[34] Y.S. Wang, C.S. Lim, C.V. Lim, M.S. Yong, E.K. Teo, L.N. Moh, In vitro degradation behavior of M1A magnesium alloy in protein-containing simulated body fluid, Mat. Sci. Eng. C Mater. 31 (2011) 579–587, https://doi.org/10.1016/j.msec.2010.11.017.

[35] Y. Wang, B.H. Ding, S.Y. Gao, X.B. Chen, R.C. Zeng, L.Y. Cui, S.J. Li, S.Q. Li, Y. H. Zou, E.H. Han, S.K. Guan, Q.Y. Liu, In vitro corrosion of pure Mg in phosphate buffer solution—influences of isoelectric point and molecular structure of amino acids[J], Mat. Sci. Eng. C Mater. 105 (2019) 110042, https://doi.org/10.1016/j.msec.2019.110042.

[36] R.Q. Hou, N. Scharnagl, F. Feyerabend, R. Willumeit-Römer, Exploring the effects of organic molecules on the degradation of magnesium under cell culture conditions, Corros. Sci. 132 (2017) 35–45, https://doi.org/10.1016/j.corsci.2017.12.023.

[37] L.X. Sun, J. Bai, F. Xue, L. Tao, C.L. Chu, J. Meng, Exceptional texture evolution induced by multi-pass cold drawing of magnesium alloy, Mater. Des. 135 (2017) 267–274, https://doi.org/10.1016/j.matdes.2017.09.027.

[38] H. Cai, J. Meng, X. Li, F. Xue, J. Bai, In vitro degradation behavior of Mg wire/poly (lactic acid) composite rods prepared by hot pressing and hot drawing, Acta Biomater. 98 (2019) 125–141, https://doi.org/10.1016/j.actbio.2019.05.059.

[39] H. Cai, Y. Zhang, J. Meng, X. Li, F. Xue, C.L. Chu, L. Tao, J. Bai, Enhanced fully-biodegradable Mg/PLA composite rod: effect of surface modification of Mg-2Zn wire on the interfacial bonding, Surf. Coat. Technol. 350 (2018) 722–731, https://doi.org/10.1016/j.surfcoat.2018.07.045.

[40] A.D. King, N. Birbilis, J.R. Scully, Accurate electrochemical measurement of magnesium corrosion rates; a combined impedance, mass-loss and hydrogen collection study, Electrochim. Acta 121 (2014) 394–406, https://doi.org/10.1016/j.electacta.2013.12.124.

[41] Y.H. Gao, A. Yerokhin, E. Parfenov, A. Matthews, Application of voltage pulse transient analysis during plasma electrolytic oxidation for assessment of characteristics and corrosion behaviour of Ca- and P-containing coatings on magnesium, Electrochim. Acta 149 (2014) 218–230, https://doi.org/10.1016/j.electacta.2014.10.063.

[42] Q.S. Dong, X.X. Zhou, Y.J. Feng, K. Qian, H. Liu, M.M. Lu, C.L. Chu, F. Xue, J. Bai, Insights into self-healing behavior and mechanism of dicalcium phosphate dihydrate coating on biomedical Mg, Bioact. Mater. 6 (2021) 158–168, https://doi.org/10.1016/j.bioactmat.2020.07.019.

[43] W. Zai, Y.C. Su, H.C. Man, J.S. Lian, G.Y. Li, Effect of pH value and preparation temperature on the formation of magnesium phosphate conversion coatings on AZ31 magnesium alloy, Appl. Surf. Sci. 492 (2019) 314–327, https://doi.org/10.1016/j.apsusc.2019.05.309.

[44] J.E. Gray-Munro, M. Strong, A study on the interfacial chemistry of magnesium hydroxide surfaces in aqueous phosphate solutions: influence of Ca2+, Cl and protein, J. Colloid Interf. Sci. 393 (2013) 421–428, https://doi.org/10.1016/j.jcis.2012.10.047.

[45] M. Kheradmandfard, M.H. Fathi, F. Ansari, T. Ahmadi, Effect of Mg content on the bioactivity and biocompatibility of Mg-substituted fluorapatite nanopowders fabricated via mechanical activation, Mat. Sci. Eng. C Mater. 68 (2016) 136–142, https://doi.org/10.1016/j.msec.2016.05.043.

[46] P.L. Jiang, R.Q. Hou, C.D. Chen, L. Sun, S.G. Dong, J.S. Pan, J.C. Lin, Controllable degradation of medical magnesium by electrodeposited composite films of mussel adhesive protein (Mefp-1) and chitosan, J. Colloid Interf. Sci. 478 (2016) 246–255, https://doi.org/10.1016/j.jcis.2016.06.001.

[47] R. Willumeit, J. Fischer, F. Feyerabend, N. Hort, U. Bismayer, S. Heidrich, B. Mihailova, Chemical surface alteration of biodegradable magnesium exposed to corrosion media, Acta Biomater. 7 (2011) 2704–2715, https://doi.org/10.1016/j.actbio.2011.03.004.

[48] H.H. Lee, M. Bae, S.H. Jo, J.K. Shin, D.H. Son, C.H. Won, J.H. Lee, Differential-mode HEMT-based biosensor for real-time and label-free detection of C-reactive protein, Sensor. Actuator. B Chem. 234 (2016) 316–323, https://doi.org/10.1016/j.snb.2016.04.117.

[49] E. Blanca, B. Torres, L.C. Maria, S. Antoine, Z. Sandrine, C. Pierangela, T. Bernard, M. Philippe, F. Isabelle, Effect of protein adsorption on the corrosion behavior of 70Cu–30Ni alloy in artificial seawater, Bioelectrochemistry 97 (2014) 34–42, https://doi.org/10.1016/j.bioelechem.2013.10.004.

[50] W. Wang, F. Mohammadi, A. Alfantazi, Corrosion behaviour of niobium in phosphate buffered saline solutions with different concentrations of bovine serum albumin, Corros. Sci. 57 (2012) 11–21, https://doi.org/10.1016/j.corsci.2011.12.039.

[51] S.L. Mcarthur, Applications of XPS in bioengineering, Surf. Interface Anal. 38 (2006) 1380–1385, https://doi.org/10.1002/sia.2498.

[52] A.P. Serro, M.P. Gispert, M.C.L. Martins, P. Brogueira, R. Colaco, B. Saramago, Adsorption of albumin on prosthetic materials: implication for tribological behavior, J. Biomed. Mater. Res. A 78 (2010) 581–589, https://doi.org/10.1002/jbm.a.30754.

[53] M. Advincula, X.W. Fan, J. Lemons, R. Advincula, Surface modification of surface sol–gel derived titanium oxide films by self-assembled monolayers (SAMs) and non-specific protein adsorption studies, Colloid. Surface. B 42 (2005) 29–43, https://doi.org/10.1016/j.colsurfb.2004.12.009.

[54] Y.S. Wang, C.S. Lim, C.V. Lim, M.S. Yong, E.K. Teo, L.N. Moh, In vitro degradation behavior of M1A magnesium alloy in protein-containing simulated body fluid, Mat. Sci. Eng. C Mater. 31 (2011) 579–587, https://doi.org/10.1016/j.msec.2010.11.017.

[55] Y. Xin, T. Hu, P.K. Chu, In vitro studies of biomedical magnesium alloys in a simulated physiological environment: a review, Acta Biomater. 7 (2011) 1452–1459, https://doi.org/10.1016/j.actbio.2010.12.004.

[56] W.D. Mueller, M.F.L. de Mele, M.L. Nascimento, M. Zeddies, Degradation of magnesium and its alloys: dependence on the composition of the synthetic biological media, J. Biomed. Mater. Res. A 90 (2009) 487–495, https://doi.org/10.1002/jbm.a.32106.

[57] A. Klinger, D. Steinberg, D. Kohavi, M.N. Sela, Mechanism of adsorption of human albumin to titanium in vitro, J. Biomed. Mater. Res. 36 (1997) 387–392, https://doi.org/10.1002/(sici)1097-4636(19970905)36:3<387::aid-jbm13>3.0.co;2-b.

[58] V. Wagener, S. Virtanen, Protective layer formation on magnesium in cell culture medium, Mat. Sci. Eng. C Mater. 63 (2016) 341–351, https://doi.org/10.1016/j.msec.2016.03.003.

[59] R. Willumeit, J. Fischer, F. Feyerabend, N. Hort, U. Bismayer, S. Heidrich, B. Mihailova, Chemical surface alteration of biodegradable magnesium exposed to corrosion media, Acta Biomater. 7 (2011) 2704–2715, https://doi.org/10.1016/j.actbio.2011.03.004.

[60] Y. Tian, L.J. Yang, Y.F. Li, Y.H. Wei, L.F. Hou, Y.G. Li, R. Murakami, Corrosion behaviour of die-cast AZ91D magnesium alloys in sodium sulphate solutions with different pH values, T. Nonferr. Metal Soc. 21 (2011) 912–920, https://doi.org/10.1016/S1003-6326(11)60801-7.

[61] R. Rettig, S. Virtanen, Composition of corrosion layers on a magnesium rare-earth alloy in simulated body fluids, J. Biomed. Mater. Res. A 88 (2010) 359–369, https://doi.org/10.1002/jbm.a.31887.